IOP Publishing Journal of Physics: Condensed Matter
J. Phys.: Condens. Matter **32** (2020) 285505 (7pp) https://doi.org/10.1088/1361-648X/ab8152

Half-metallic two-dimensional polyaniline with 3d-transition-metal decoration

Zhongyao Li and Min Chen

College of Science, University of Shanghai for Science and Technology, Shanghai 200093, People's Republic of China

E-mail: lizyusst@gmail.com

Received 3 January 2020, revised 7 March 2020
Accepted for publication 19 March 2020
Published 17 April 2020

Abstract

Possible half-metallic behavior was explored in 3d-transition-metal (Fe, Co, and Ni) decorated two-dimensional polyaniline (C_3N) on the basis of density-functional theory. 3d-transition-metal atoms would prefer to adsorb on top of the carbon hexagonal ring. The calculated electronic structures suggest the Fe and Co decorated polyanilines ($(C_3N)_2Fe$ and $(C_3N)_2Co$) are magnetic half-metals, while the Ni-decorated polyaniline ($(C_3N)_2Ni$) is a nonmagnetic semiconductor with an enlarged band gap. In $(C_3N)_2Fe$, the half-metallic energy window can be as large as 0.7 eV. Interestingly, there are two half-metallic energy windows with opposite spins near Fermi level in $(C_3N)_2Co$. The energy windows and band gaps can be modulated by the distance between 3d-transition-metal atoms and C_3N. Due to the large half-metallic energy window and the appropriate band gap, 3d-transition-metal decorated C_3N may be used in nanoscale spintronic devices.

Keywords: half-metal, first-principles calculation, two-dimensional polyaniline, band structure

(Some figures may appear in colour only in the online journal)

1. Introduction

Two-dimensional (2D) material has been one of the fundamental fields of materials [1–7]. Interestingly, one kind of 2D material is comprised of C and N atoms, such as $C_{12}N$, g-C_4N_3, C_3N, etc [8–12]. Among these 2D carbonitrides, 2D polyaniline (C_3N) has a graphene-like honeycomb structure and has been widely studied due to the unique physical and chemical properties [13, 14]. Theoretically, this novel 2D material can yield ultra-high stiffness, superior stability, and thermal conductivity [15, 16]. It may be employed in solar cell devices, electrolyte gating and anode materials [17–19]. Moreover, it may have great potential applications in high-performance electronic devices due to its appropriate band gap, high carrier mobility and high on–off current ratio [20]. Single-layer C_3N was first proposed in theory with special methods and techniques [21], and then synthesized successfully in experiments [20, 22, 23]. Its primitive cell is comprised of six C atoms and two N atoms. It can be regarded as a graphene-like structure with 25% N-doping in graphene [24]. Single-layer C_3N is a semiconductor, while three-layer C_3N becomes metal [25]. Therefore, semiconductor–metal nanostructure can be constructed through seamless joining of single-layer and multilayer polyaniline.

The properties of C_3N can be improved or tuned by adatom adsorption, doping, defect, adding an electric field, stress change or other methods [26–34]. Qin *et al* studied the adsorption of CO_2 on monolayer polyaniline [35]. By changing the electric field and the charge of the adsorption system, C_3N can capture and release CO_2. It was also studied that the effect of defect, strain and electric field on the adsorption of CO_2 [36]. 2D polyaniline can also exhibit different properties when it is doped by different atoms, especially for the doping of 3d-transition-metals (3d-TMs) [19, 37]. Magnetism can be realized in the C_3N with adsorption of most 3d-TM adatoms [19, 31, 38], which may be utilized in spintronics.

In this work, we studied the electronic structures of 3d-TM decorated single-layer polyaniline and explored the possible half-metallic behavior in the systems. Half-metallic material is a new type of functional electronic material, which has

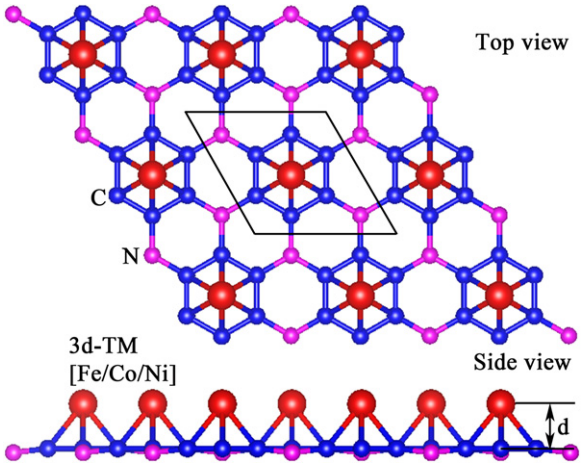

Figure 1. Top and side views of the structure of the 3d-TM (Fe, Co or Ni) decorated C_3N. The black rhombus represents the primitive cell of the system. 3d-TM atoms prefer to adsorb on top of the carbon hexagonal ring in C_3N. The lattice constant is set to be 4.86 Å. It is denoted as *d* that the distance between the 3d-TM atoms and the hexagonal carbon ring of C_3N.

special spin-polarized band structures and good potentials for applications in nanoscale spintronic devices. It can produce perfect spin-polarized carriers and is very suitable as a spin-injected source material [39–41]. Our calculations indicate half-metal behavior may be realized in Fe and Co decorated C_3N ($(C_3N)_2Fe$ and $(C_3N)_2Co$) in relatively large energy windows near Fermi level, while the Ni-decorated C_3N ($(C_3N)_2Ni$) is a nonmagnetic semiconductor with an enlarged band gap. Moreover, the half-metallic conduction band of $(C_3N)_2Fe$ has spin-polarized free-electron-like electronic structure with a relatively small effective mass. Therefore, Fe-decorated 2D polyaniline may be a more practicable half-metal in spintronics.

2. Method and computational details

Based on the spin-polarized density functional theory (DFT), first-principles calculations were carried out using the Vienna *ab initio* simulation package (VASP) [42] with the projector-augmented wave (PAW) method [43]. The electronic exchange–correlation potential was treated by the generalized gradient approximation (GGA) [44] with the Perdew–Burke–Ernzerhof (PBE) method [45]. The DFT-D2 method was used to describe the van der Waals interaction [46]. By the PBE method, the calculated band gap of single-layer C_3N is about 0.39 eV, which is consistent with the reported result in experiment [20]. Therefore, we mainly used the PBE method in this work. As a comparison, we also calculated the band structures of the stable 3d-TM decorated C_3N by the Heyd–Scuseria–Ernzerhof (HSE06) method [47], which is known to be usually more accurate than the PBE method [48].

In our calculations, the energy cutoff was set to be 500 eV, and the total energy was converged to better than 10^{-6} eV. All the calculations are spin dependent. The majority (minority) spin is set to be up-spin (down-spin). The equilibrium structures were obtained through structural relaxation until

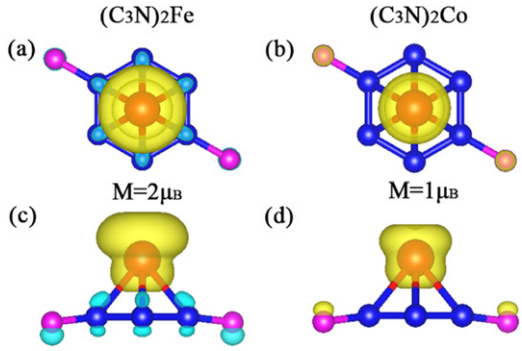

Figure 2. Top views (a, b) and side views (c, d) of the distribution of spin-charge density in $(C_3N)_2Fe$ (a, c) and $(C_3N)_2Co$ (b, d). The up-spin and down-spin are marked in yellow and cyan, respectively. The isosurface contour is set to be 0.005 e $Å^{-3}$.

Hellmann–Feynman forces were less than 0.001 eV $Å^{-1}$. The structures were modeled by periodic slabs geometry with a vacuum of 20 Å in the *z*-direction. The Γ-centered *k*-point grid of $15 \times 15 \times 1$ was used for Brillouin zone sampling in all calculations except for the calculation of density of states (DOS). For the calculation of DOS, the number of *k*-points is increased to $21 \times 21 \times 1$.

The lattice constant of C_3N is set to be 4.86 Å [20, 23], and both the C–C and C–N bond length are about 1.40 Å [49]. The structure of C_3N changes a little when it is decorated by 3d-TM (Fe, Co, and Ni) atoms. In the 3d-TM decorated C_3N, the nitrogen atoms and the carbon atoms are not in the same plane. Therefore, corrugation of the C_3N plane can be found due to the displacement of the nitrogen atoms with respect to the carbon atoms. Although a small corrugation of the C_3N plane is induced by the 3d-TM atoms, the lattice constant changes little. For the 3d-TM decorated C_3N, each C_3N cell is decorated by one 3d-TM atom. Therefore, the 3d-TM decorated C_3N can be denoted as $(C_3N)_2TM$ (TM = Fe, Co or Ni). The binding energy between C_3N and 3d-TM atom is defined as $E_b = E_{C_3N} + E_{TM} - E_{(C_3N)_2TM}$, where E_{C_3N}, E_{TM}, and $E_{(C_3N)_2TM}$ are the total energies of the C_3N cell, the isolated 3d-TM atom, and the 3d-TM decorated C_3N cell, respectively. Larger binding energy represents more stable decoration and stronger TM–C_3N interaction.

3. Results and discussion

Although several initial positions of 3d-TM atoms are considered, 3d-TM atoms would prefer to adsorb on top of the hexagonal carbon ring in C_3N. It is consistent with the reported results [19]. Figure 1 shows the structure of the 3d-TM decorated C_3N. Decoration of 3d-TM atoms induces a small corrugation of C_3N plane. At equilibrium, the induced corrugation is about 0.15 Å, 0.16 Å, and 0.20 Å in $(C_3N)_2$ Fe, $(C_3N)_2Co$, and $(C_3N)_2Ni$, respectively. The distance between 3d-TM atoms and C_3N (hexagonal carbon ring) is about 1.55 Å, 1.52 Å, and 1.53 Å for the Fe, Co, and Ni atoms, respectively. Despite the fact that the TM–C_3N distance is very close to each other, their binding energies are different. The binding energy of $(C_3N)_2$ Fe/Co/Ni is about 1.59 eV, 1.75 eV,

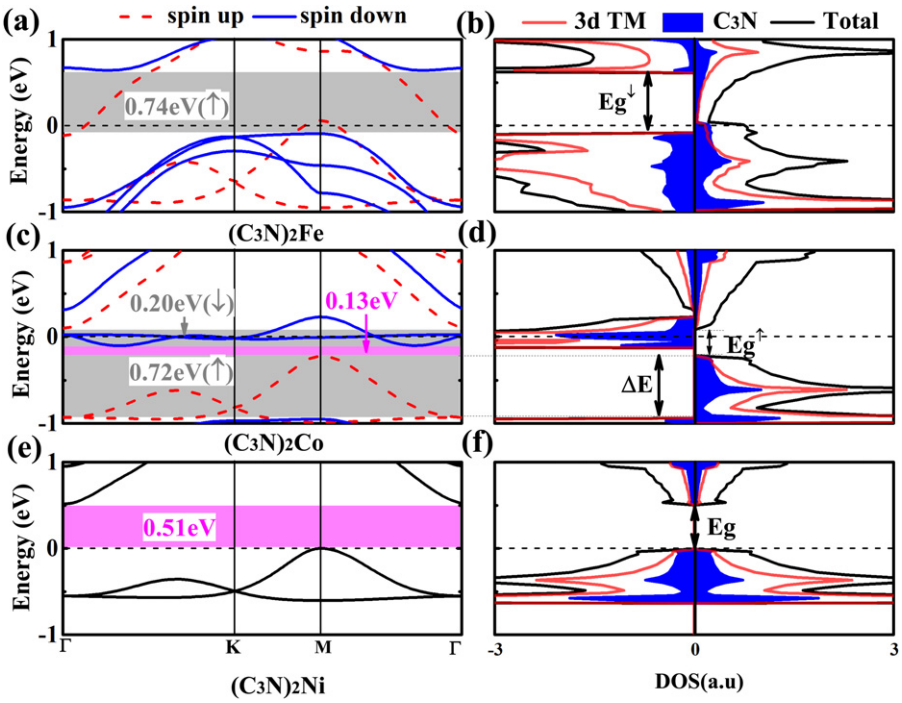

Figure 3. Band structures (a, c, and e) and density of states (DOS) (b, d, and f). In figures (a), (c) and (e), the half-metallic energy windows are highlighted in gray. The band gap of semiconductor is marked in pink in figures (c) and (e). In figure (b), the band gap of down-spin is denoted as $E_g^{\downarrow}$. In figure (d), the band gap of up-spin is denoted as $E_g^{\uparrow}$ and the half-metallic energy window with up-spin-polarized band is denoted as ΔE. In figure (f), the band gap is denoted as E_g. The Fermi level is set to be zero.

and 2.13 eV, respectively. The larger Ni–C_3N binding energy suggests the stronger Ni–C_3N interaction. Among the three 3d-TM decorated structures, $(C_3N)_2Fe$ and $(C_3N)_2Co$ are magnetic. The magnetic moments of $(C_3N)_2Fe$ and $(C_3N)_2Co$ are about 2 μ_B and 1 μ_B each cell, respectively. Figure 2 shows the distribution of spin-charge density in $(C_3N)_2Fe$ and $(C_3N)_2Co$. The magnetism is mainly from the 3d-TM atoms in both systems, and the C_3N is weakly magnetized. In $(C_3N)_2Fe$, the C_3N has opposite weak magnetism to that of Fe atoms. The magnetic moments of Fe atoms and C_3N are about 1.90 μ_B (spin-up) and 0.14 μ_B (spin-down), respectively. Differently, only the N atoms are weakly magnetized in $(C_3N)_2Co$. The magnetic moments of Co and N atoms are about 0.93 μ_B (spin-up) and 0.03 μ_B (spin-up), respectively. Besides, the total energy of magnetic $(C_3N)_2Fe$ and $(C_3N)_2Co$ is about 1.43 eV and 0.11 eV lower than that of non-magnetic states, respectively. The values are significantly higher than the thermal excitation energy of 26 meV at room temperature. Therefore, both magnetic systems may exist at room temperature.

Figure 3 shows the band structures and the density of states (DOS) in the 3d-TM decorated polyanilines. Interesting half-metallic property can be found in magnetic $(C_3N)_2Fe$ and $(C_3N)_2Co$. The Fe-decorated polyaniline is a semiconductor for down-spin with a band gap of about 0.74 eV, while it is a metal for up-spin. In $(C_3N)_2Fe$, the half-metallic energy window is about (−0.10 eV, 0.64 eV), i.e. from −0.10 eV to 0.64 eV. In this range, there are only up-spin-polarized bands. The energy window is also the band gap of down-spin ($E_g^{\downarrow}$ in figure 3(b)). In this range (the down-spin band gap), the DOS of conduction band is partly from the C_3N and the Fe atoms. The limited contribution of C_3N and Fe atoms to the DOS suggests the conduction band has spin-polarized free-electron-like electronic structure. The calculated effective mass is about $0.4m_e$, which is comparable to the effective mass in C_3N [50–52]. The relatively small Fe–C_3N binding energy suggests a weaker Fe–C_3N interaction, which may lead to a weaker constraint of electrons. The half-metallic property can also be found in the Co-decorated polyaniline. Differently, the band gap of up-spin band ($E_g^{\uparrow}$ in figure 3(d)) is from −0.23 eV to 0.10 eV, about 0.33 eV in $(C_3N)_2Co$, while the down-spin-polarized bands are metallic. The band gap of up-spin is close to the band gap of C_3N. Interestingly, there are two half-metallic energy windows with opposite spins near Fermi level. One is from −0.10 eV to 0.10 eV, in which there are only down-spin-polarized bands. The size is about 0.20 eV. Another is from −0.95 eV to −0.23 eV, in which there are only up-spin-polarized bands. It is denoted as ΔE in figure 3(d). The size is about 0.72 eV. The energy windows are different from the band gaps. The gap between the two ranges is about 0.13 eV. From the DOS, the half-metallic properties for both spins are induced by the hybridization of C_3N and Co atoms. However, the down-spin-polarized conduction band has a narrow bandwidth. It is just like an impurity band in the band gap of up-spin. In fact, there is a down-spin-polarized flat band at Fermi level. It suggests the down-spin-polarized states are relatively localized near Fermi level, which may be concerned with the relatively strong Co–C_3N interaction. The nonmagnetic $(C_3N)_2Ni$ is a semiconductor. Despite the fact that the valence band is also from the hybridization of C_3N and Ni atoms, its conduction band has limited components from the

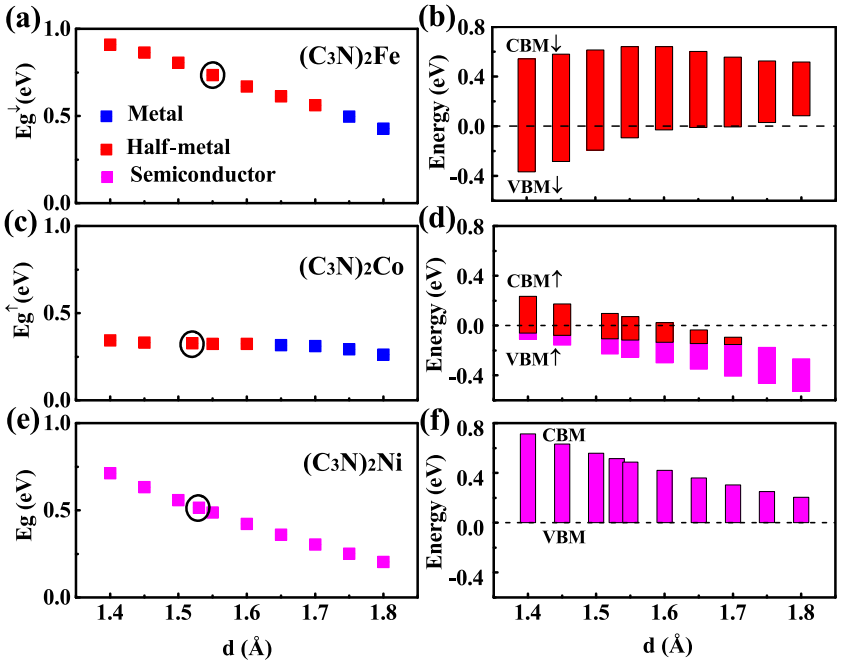

Figure 4. The (spin dependent) band gaps (a, c, and e) and the corresponding energies of CBM and VBM (b, d and f) as functions of the TM–C_3N distance (d). The band gap of down-spin in $(C_3N)_2Fe$ [$E_g^{\downarrow}$ in figure (a)], the band gap of up-spin in $(C_3N)_2Co$ [$E_g^{\uparrow}$ in figure (c)] and the band gap in $(C_3N)_2Ni$ [E_g in figure (e)] are also marked in figures 3(b), (d) and (f), respectively. The equilibrium band gaps are marked in black circles. The Fermi level is set to be zero. In figures (b), (d), and (f), the lateral size of rectangles is meaningless. It is used only for visual effect.

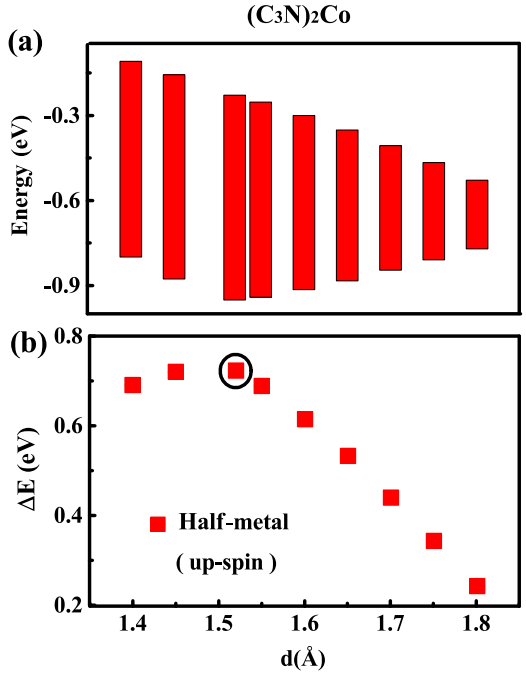

Figure 5. (a) The half-metallic energy window in $(C_3N)_2Co$ for up-spin. (b) The size of the window. It is also denoted as ΔE in figure 3(d). The equilibrium result is marked in black circle. The Co–C_3N distance is denoted as d. In figure (a), the lateral size of rectangles is meaningless. It is used only for visual effect.

C_3N and Ni atoms. The band gap of $(C_3N)_2Ni$ is enlarged to be about 0.51 eV, compared with the band gap of C_3N (about 0.39 eV). This result appears to be strange since metallic atoms usually contribute to metallic properties. The enlarged band gap may be concerned with the strong Ni–C_3N interaction, which may trap electrons as covalent bonds.

Since the half-metallic property is from the TM–C_3N interaction, the half-metallic energy windows and the (spin dependent) band gaps should be varied by straining the distance between 3d-TM atoms and C_3N. Therefore, we studied the influence of the distance on the electronic structures of systems. The results are shown in figures 4 and 5. Figure 4 shows the (spin dependent) band gaps (figures 4(a), (c) and (e)) and the corresponding energies of CBM and VBM (figures 4(b), (d) and (f)) as functions of the TM–C_3N distance (d). In $(C_3N)_2Fe$ (figure 4(a) and (b)), the band gap of down-spin linearly decreases with the increase of the Fe–C_3N distance. Meanwhile, in $(C_3N)_2Fe$ (figure 4(b)), the half-metallic property can still be found in the whole band gap. The decrease of the band gap is mainly caused by the increase of the valence band maximum (VBM) of down-spin, while the conduction band minimum (CBM) of down-spin has only a slight change. When the distance is larger than 1.7 Å, the VBM of down-spin would be above the Fermi level. The half-metallic property would disappear at Fermi level in this case. The results also suggest the energy window of half-metal can be further enlarged by decreasing the Fe–C_3N distance. Therefore, the half-metallic property can be further enhanced in $(C_3N)_2Fe$. Differently, the band gap of up-spin is insensitive to the distance in $(C_3N)_2Co$ (figure 4(c) and (d)). However, the half-metallic window in the band gap decreases by enlarging the distance. When the distance is larger than 1.6 Å, the CBM of up-spin would be below the Fermi level and the half-metallic property disappears at Fermi level. Furthermore, the half-metallic window would disappear

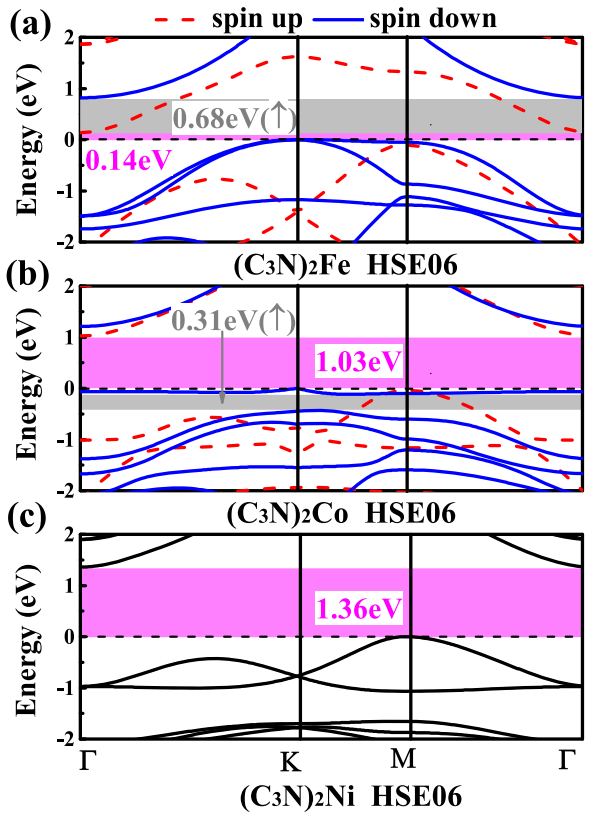

Figure 6. The band structures of the stable $(C_3N)_2Fe$ (a), $(C_3N)_2Co$ (b) and $(C_3N)_2Ni$ (c) by the HSE06 method, respectively. In figures (a) and (b), the half-metallic energy windows are highlighted in gray. The band gap of semiconductor is marked in pink. The Fermi level is set to be zero.

when the distance is larger than 1.7 Å. As for the band gap of $(C_3N)_2Ni$ (figure 4(e) and (f)), it linearly decreases with the increase of the Ni–C_3N distance due to the weakening of the Ni–C_3N interaction.

Another half-metallic energy window, which is denoted as ΔE in figure 3(d), can also be modulated by the Co–C_3N distance in $(C_3N)_2Co$. At equilibrium, the energy window is from −0.95 eV to −0.23 eV. The size is about 0.72 eV. In this range, there are only up-spin-polarized bands. With the increase of the Co–C_3N distance, the energy window would be linearly reduced as shown in figure 5. Since the energy window is from the hybridization of C_3N and Co atoms, it would disappear when the distance is large enough.

As a comparison, we calculated the band structures of the stable 3d-TM decorated polyanilines by the HSE06 method. The results are shown in figure 6. Although the Fe-decorated polyaniline becomes a magnetic semiconductor, the band gap is only about 0.14 eV (figure 6(a)). Moreover, a large half-metallic energy window can still be found. The energy window is from about 0.14 eV to 0.82 eV. The size is about 0.68 eV, which is comparable with that from the PBE method. Therefore, the half-metallic property appears to be stable and credible in $(C_3N)_2Fe$. The Co-decorated polyaniline also becomes a magnetic semiconductor. However, its band gap is much larger, which is about 1.03 eV (figure 6(b)). As above mentioned, there are two half-metallic energy windows with opposite spins in $(C_3N)_2$ Co from the PBE method. The HSE06 method reduces the two energy windows. One disappears, another window changes to be about (−0.43 eV, −0.12 eV). The up-spin-polarized half-metallic range is only about 0.31 eV. Therefore, the half-metallic property may need to be further explored in $(C_3N)_2Co$ due to the different results from PBE and HSE06 methods. Finally, compared with the PBE result, the HSE06 method enlarges the band gap of $(C_3N)_2Ni$ from 0.51 eV to 1.36 eV (figure 6(c)), which is also larger than the band gap of C_3N by the HSE06 method (1.04 eV). Therefore, it would be credible that the Ni-decoration can enlarge the band gap of C_3N due to the consistent results from PBE and HSE06 methods. The larger band gap may suggest strong and localized Ni–C_3N interaction.

4. Conclusion

In summary, we investigated the electronic structures of 3d-TM decorated polyanilines and the half-metallic property in the systems. Both $(C_3N)_2Fe$ and $(C_3N)_2Co$ are magnetic half-metals by the PBE calculations. The half-metallic ranges can be as large as 0.7 eV near Fermi level. Although the HSE06 method suggests $(C_3N)_2Fe$ is a semiconductor, the band gap is relatively small and a large half-metallic energy window can still be found near Fermi level. Therefore, the half-metallic property appears to be stable and credible in $(C_3N)_2$ Fe. However, the half-metallic property may need to be further explored in $(C_3N)_2Co$. The Ni-decorated polyaniline is a nonmagnetic semiconductor. Strangely, the band gap of $(C_3N)_2Ni$ is larger than that of C_3N, it may be induced by the strong and localized Ni–C_3N interaction. The half-metallic energy windows and the (spin dependent) band gaps can be modulated by the distance between 3d-TM atoms and C_3N. Due to the special electronic structures and half-metallic properties, these 3d-TM decorated C_3N may be used in nanoscale spintronic devices.

Acknowledgments

This work was supported by the National Natural Science Foundation of China under Grant No. 11204178. The authors also thank the support from the University of Shanghai for Science and Technology (Science and Technology Development Project) under Grant No. 2017KJFZ115.

ORCID iDs

Zhongyao Li https://orcid.org/0000-0002-3295-7718

References

[1] Elemans J A A W, Lei S and De Feyter S 2009 Molecular and supramolecular networks on surfaces: from two-dimensional crystal engineering to reactivity *Angew. Chem., Int. Ed.* **48** 7298–332

[2] Balandin A A, Ghosh S, Bao W, Calizo I, Teweldebrhan D, Miao F and Lau C N 2008 Superior thermal conductivity of single-layer graphene *Nano Lett* **8** 902–7

[3] Novoselov K S, Jiang D, Schedin F, Booth T J, Khotkevich V V, Morozov S V and Geim A K 2005 Two-dimensional atomic crystals *Proc. Natl. Acad. Sci. USA* **102** 10451–3

[4] Alarcon-Angeles G, Palomar-Pardave M and Merkoci A 2018 2D materials-based platforms for electroanalysis applications *Electroanalysis* **30** 1271–80

[5] Zhao W, Liu J C, Ding Z X, Zhang J H and Wang X Y 2020 Optimal synthesis of platinum-free 1D/2D CdS/MOS_2 (CM) heterojunctions with improved photocatalytic hydrogen production performance *J. Alloys Compd.* **813** 152234

[6] Ming X 2018 A review on applications of two-dimensional materials in surface-enhanced raman spectroscopy *Int. J. Spectrosc.* **2018** 1–9

[7] Yue Y L, Jiang C, Han Y L, Wang M, Ren J and Wu Y K 2020 Magnetic anisotropies of Mn-, Fe-, and Co-doped monolayer MoS_2 *J. Magn. Magn. Mater.* **496** 165929

[8] Matar S F 2019 Magnetization on nitrogen in extended honeycomb carbon layers from first principles: case studies of C_xN (x = 2, 6, 12) *J. Magn. Magn. Mater.* **469** 46–51

[9] Zhou X, Li F, Xing Y and Feng W 2019 Multifield-tunable magneto-optical effects in electron- and hole-doped nitrogen-graphene crystals *J. Mater. Chem.* C **7** 3360–8

[10] Zhu J, Zhang S Y, Zechel D L, Paululat T and Bechthole A 2019 Rational design of hybrid natural products by utilizing the promiscuity of an amide synthetase *ACS Chem. Biol.* **14** 1793–801

[11] Huang W C, Li W and Liu X 2018 Exotic ferromagnetism in the two-dimensional quantum material C_3N *Front. Phys.* **13** 137104

[12] Li L, Kong X, Leenaerts O, Xin C, Sanyal B and Peeters F M 2017 Carbon-rich carbon nitride monolayers with Dirac cones: Dumbbell C_4N *Carbon* **118** 285–90

[13] Kumar S, Sharma S, Babar V and Schwingenschlögl U 2017 Ultralow lattice thermal conductivity in monolayer C_3N as compared to graphene *J. Mater. Chem.* A **5** 20407–11

[14] Wang D W *et al* 2009 Fabrication of graphene/polyaniline composite paper via *in situ* anodic electropolymerization for high-performance flexible electrode *ACS Nano* **3** 1745–52

[15] Mortazavi B 2017 Ultra high stiffness and thermal conductivity of graphene like C_3N *Carbon* **118** 25–34

[16] Hong Y, Zhang J and Zeng X C 2018 Monolayer and bilayer polyaniline C_3N: two-dimensional semiconductors with high thermal conductivity *Nanoscale* **10** 4301–10

[17] Chang M-Y, Wu C-S, Chen Y-F, Hsieh B-Z, Huang W-Y, Ho K-S, Hsieh T-H and Han Y-K 2008 Polymer solar cells incorporating one-dimensional polyaniline nanotubes *Org. Electron.* **9** 1136–9

[18] Alam M M, Wang J, Guo Y, Lee S P and Tseng H-R 2005 Electrolyte-gated transistors based on conducting polymer nanowire junction arrays *J. Phys. Chem.* B **109** 12777–84

[19] Bafekry A, Shayesteh S F and Peeters F M 2019 C_3N monolayer: Exploring the emerging of novel electronic and magnetic properties with adatom adsorption, functionalizations, electric field, charging, and strain *J. Phys. Chem.* C **123** 12485–99

[20] Yang S *et al* 2017 C_3N: a 2D crystalline, hole-free, tunable-narrow-bandgap semiconductor with ferromagnetic properties *Adv. Mater.* **29** 1605625

[21] Zhou X, Feng W, Guan S, Fu B, Su W and Yao Y 2017 Computational characterization of monolayer C_3N: a two-dimensional nitrogen-graphene crystal *J. Mater. Res.* **32** 1–9

[22] Mahmood J *et al* 2016 Two-dimensional polyaniline (C_3N) from carbonized organic single crystals in solid state *Proc. Natl. Acad. Sci. USA* **113** 7414

[23] Mortazavi B 2017 Ultra high stiffness and thermal conductivity of graphene like C_3N *Carbon* **118** 25–34

[24] Zhiming S, Alex K and Yakobson B I 2015 How much N-doping can graphene sustain? *J. Phys. Chem. Lett.* **6** 106–12

[25] Li W F, Dai X, Morrone J, Zhang G and Zhou R H 2017 Thickness dependent semiconductor-to-metal transition of two-dimensional polyaniline with unique work functions *Nanoscale* **9** 12025–31

[26] Yu Y, Fu H, She L, Lu S, Guo Q, Li H, Meng S and Cao G 2017 Fe on Sb(111): potential two-dimensional ferromagnetic superstructures *ACS Nano* **11** 2143–9

[27] Rasool H I, Ophus C and Zettl A 2015 Atomic defects in two dimensional materials *Adv. Mater.* **27** 5771–7

[28] Xie L, Yang L, Ge W, Wang X and Jiang J 2019 Bandgap tuning of C_3N monolayer: A first-principles study *Chem. Phys.* **520** 40–6

[29] Yang B and Fu Z 2019 Comparative study of C_3N- and graphene-supported single-atom Pt *J. Phys. Chem.* C **123** 5731–5

[30] Guo G C, Wang R Z, Ming B M, Wang C, Luo S W, Lai C and Zhang M 2019 Trap effects on vacancy defect of C_3N as anode material in Li-ion battery *Appl. Surf. Sci.* **475** 102–8

[31] Makaremi M, Mortazavi B and Singh C V 2017 Adsorption of metallic, metalloidic and nonmetallic adatoms on two-dimensional C_3N *J. Phys. Chem.* C **121** 18575–83

[32] Tian L L, Yang J, Weng M Y, Tan R, Zheng J X, Chen H B, Zhuang Q C, Dai L M and Pan F 2017 Fast diffusion of O_2 on nitrogen-doped graphene to enhance oxygen reduction and its application for high-rate Zn-air batteries *ACS Appl. Mater. Interfaces* **9** 7125–30

[33] Zhao Y M, Ma D W, Zhang J, Lu Z S and Wang Y X 2019 Transition metal embedded C_3N monolayers as promising catalysts for the hydrogen evolution reaction *Phys. Chem. Chem. Phys.* **21** 20432–41

[34] Zhou Y, Gao G, Kang J, Chu W and Wang L 2019 Transition metal embedded two-dimensional C_3N as highly active electrocatalysts for oxygen evolution and reduction reactions *J. Mater. Chem.* A **7** 12050–9

[35] Qin G Q, Cui Q Y, Wang W H, Li P, Du A J and Sun Q 2018 First-principles study of electrocatalytically reversible CO_2 capture on graphene-like C_3N *Chemphyschem* **19** 2788–95

[36] Li X F, Guo T C, Zhu L, Ling C C, Xue Q Z and Xing W 2018 Charge-modulated CO_2 capture of C_3N nanosheet: insights from DFT calculations *Chem. Eng. J.* **338** 92–8

[37] Yang T T, Huang Y, Yang L, Li X Y, Wang X J, Zhang G Z, Luo Y and Jiang J 2019 Protecting single atom catalysts with graphene/carbon-nitride 'Chainmail' *J. Phys. Chem. Lett.* **10** 3129–33

[38] Zhou Y N, Gao G P, Kang J, Chu W and Wang L W 2019 Transition metal-embedded two-dimensional C_3N as a highly active electrocatalyst for oxygen evolution and reduction reactions *J. Mater. Chem.* A **7** 12050–9

[39] Li Z Y, Xie W Z, Liu X G and Wu Y 2015 Magnetic property and possible half-metal behavior in Co-doped graphene *J. Appl. Phys.* **117** 5

[40] Tagani M B and Vishkayi S I 2018 Polyaniline (C_3N) nanoribbons: magnetic metal, semiconductor, and half-metal *J. Appl. Phys.* **124** 084304

[41] Guan Z, Wang J, Huang J, Wu X, Li Q and Yang J 2014 Metal-free magnetism and half-metallicity of carbon nitride nanotubes: a first-principles study *J. Phys. Chem.* C **118** 22491–8

[42] Kresse G and Furthmller J 1996 Efficiency of *ab-initio* total energy calculations for metals and semiconductors using a plane-wave basis set *Comput. Mater. Sci.* **6** 15–50

[43] Blöchl P E 1994 Projector augmented-wave method *Phys. Rev.* B **50** 17953–79

[44] Perdew J P, Burke K and Ernzerhof M 1996 Generalized gradient approximation made simple *Phys. Rev. Lett.* **77** 3865–8

[45] Perdew J P, Ernzerhof M and Burke K 1996 Rationale for mixing exact exchange with density functional approximations *J. Chem. Phys.* **105** 9982–5

[46] Grimme S 2006 Semiempirical GGA-type density functional constructed with a long-range dispersion correction *J. Comput. Chem.* **27** 1787–99
[47] Vydrov O A and Scuseria G E 2006 Assessment of a long-range corrected hybrid functional *J. Chem. Phys.* **125** 234109
[48] Heyd J, Scuseria G E and Ernzerhof M 2003 Hybrid functionals based on a screened coulomb potential *J. Chem. Phys.* **118** 8207–15
[49] Babar V, Sharma S and Schwingenschlögl U 2018 Highly sensitive sensing of NO and NO_2 gases by monolayer C_3N *Adv. Theory Simul.* **1** 1700008
[50] Shi L-B, Zhang Y-Y, Xiu X-M and Dong H-K 2018 Structural characteristics and strain behaviors of two-dimensional C_3N: first principles calculations *Carbon* **134** 103–11
[51] Wang X, Li Q, Wang H, Gao Y, Hou J and Shao J 2018 Anisotropic carrier mobility in single- and bi-layer C_3N sheets *Physica* B **537** 314–9
[52] Li Z M, Yao Y P, Wang T Y, Lu K, Zhang P, Zhang W and Yin J R 2019 Electronic properties of two-dimensional IV-V group materials from density functional theory *Appl. Surf. Sci.* **496** 143730